Electronic Supplementary Material (ESI) for Nanoscale.

Fabrication of Pixelated Liquid Crystal Nanostructures Employing the Contact Line Instabilities of Droplets

Bolleddu Ravi,[a] Mitradip Bhattacharjee,[b] Abir Ghosh[b] and Dipankar Bandyopadhyay*[a,b]

[a]Department of Chemical Engineering, Indian Institute of Technology Guwahati, 781039 - India.

[b]Centre for Nanotechnology, Indian Institute of Technology Guwahati, 781039 - India.

†**Corresponding author**. Dipankar Bandyopadhyay, Centre for Nanotechnology and Department of Chemical Engineering, Indian Institute of Technology Guwahati, 781039 - India. Email: dipban@iitg.ernet.in

I. Lorentz Force Experiment

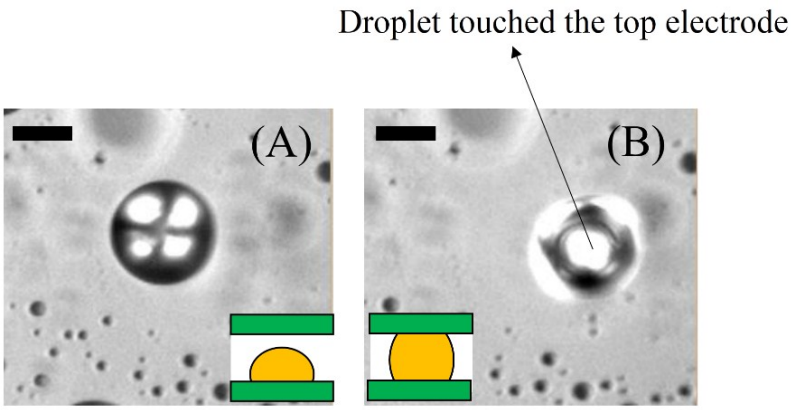

Figure S1: The figure shows the microscopic images of the 5CB droplet in the experimental setup for the Lorentz force (A) before and (B) after touching the top electrode. The inset diagrams at the bottom of each image show the schematic illustration of the set-up at the respective conditions. The scale bars in this case are of 20 μm.

Figure S1 shows the microscopic images of the 5CB droplet before and after touching the top electrode.

II. Variation in Surface Tension: Marangoni Flows

The solvent penetrated through the film matrix owing to the concentration gradient. In such systems the temperature variation was expected to be marginal and hence the thermal Marangoni flow was neglected. In fact, during the evaporation of the solvent from the film matrix, there could be a significant variation in temperature. However, again this gradient would be vertical rather than across the film-air interface, which might not lead to thermal Marangoni flows.

However, a marginal variation in the thickness of a thin film was omnipresent across the radial direction because of the presence of the random perturbations or fluctuations in the environment. In such situation, solvent was assumed to evaporate to the ambient atmosphere. Although, such solvent evaporation could be a fairly uniform process, the variation in height would induce lateral variation in surface tension across the evaporating interface. Specifically, the the thinner (thicker) film regions changed composition faster (slower) because of the relatively rapid (sluggish) evaporation of the solvent from the film, which could lead to the solutal Marangoni flows. The composition variation across the film was the main cause for the development of the surface tension gradient across the interface. Thus, we modelled the variation in the surface tension in terms of local concentration $C(r,t)$ as, $\gamma(r) = \gamma_{ps} + mC(r,t)$ where $C(r,t)$ is fractional LC concentration $[LC/(LC+S)]$ in the solution, γ_{ps} is the surface tension of the pure solvent, and m is the slope of the surface tension with 5CB liquid crystal concentration. This slope can be positive or negative conditional on the system.

Experimentally, it was difficult to measure the real time change in the surface tension during the evaporation. In order to represent the variation in the surface tension we used the abovementioned 1st order model, which was capable of capturing this variation in surface tension

because of composition variation. This model is also used previously for similar kind of systems as discussed in **Ref. 59** of the main manuscript. In this model, we tried to capture the variation of surface tension in (r,t) via film composition $C(r,t)$ and the slope m. The film composition, $C(r,t)$, was again modelled using initial concentration and initial film height as, $C(r,t)h_0 = C_i h_i$ [**Ref. 58** of the main manuscript], which were easy to obtain from the experiments. Initial concentration of 5CB liquid crystal (C_i) was calculated from the ratio of amount of 5CB droplet dispensed on the PDMS substrate to the total amount of 5CB and n-hexane added to the system, initially ($t = 0$). Initial drop height used as initial film thickness. The effect of the slope, m, also investigated and considered accordingly. For the present study, $m = 0.1$, was found to be in good agreement with the experimental results. We overcame the shortcoming of the real time measurement of the variable surface tension across the interface (r,t) using the abovementioned methodology.

III. Hamaker Constants

The system considered in the manuscript was a thin film composed of 5CB liquid crystal and n-hexane on PDMS substrate. The solvent n-hexane was loaded with a very small amount of 5CB ($C_i = 0.01$). So, the Hamaker constant of n-hexane was considered as the film Hamaker constant. In the theoretical analysis, effective Hamaker constant (A_e) was calculated using binary Hamaker constants as, $A_e = A_{ff} - A_{sf}$ [**Ref. 66** of the main manuscript]. The subscripts, f and s denote the thin film (n-hexane) and substrate (PDMS), respectively. Hamaker constant of n-hexane is, $A_{ff} = 4.1 \times 10^{-20}$ J [**Ref. 67** of the main manuscript] and the same for PDMS is, $A_{ss} = 4.4 \times 10^{-20}$ J [**Ref. 68** of the main manuscript]. The binary Hamaker constant is, $A_{sf} = (A_{ss}A_{ff})^{1/2} = 4.3 \times 10^{-20}$ J, which leads to the effective Hamaker constant, $A_e = A_{ff} - A_{sf} = -0.2 \times 10^{-20}$ J.

Description of the Supporting Videos

Supporting video 1: The video shows solvent vapor induced generation of 5CB microdroplets on a homogeneous hydrophobic PDMS substrate when the initial drop diameter was 36 ± 0.5 μm. Initially, the solvent diffusion into the droplet matrix led to the NI transition before the drop started spreading. The convex meniscus of the droplet shrunk from 36 ± 0.5 μm to 23 ± 0.5 μm after t = 2.36 min, which further reduced to about 8 ± 0.08 μm after t = 3.36 min. Although the dissolution of the droplet meniscus was visible in the optical images, the spreading of the contact line and the formation of the non-uniform film were beyond the limit of optical characterization.

Supporting video 2: The video shows solvent vapor induced generation of 5CB microdroplets on a homogeneous hydrophobic PDMS substrate when the initial drop diameter was 167 ± 1 μm. The droplet retained its lens like convex meniscus while expanding to form a non-uniform film, with the progressive expansion of contact-line and reduction of the contact angle

with time. The spreading of the droplet with the convex meniscus had diameter of 372 ± 0.54 μm after t = 10.45 min and 697±0.36 μm after t = 13 min.

Supporting video 3: The video shows micro/nano droplets generation with initial drop diameter 246 ± 1 μm. Initially the drop was in nematic state as could be followed by the cross polarized microscopy (inset). When the drop was exposed to solvent vapor at t = 0 s, the vapor penetration into the drop cause NI transition, after, t = 0.2 min. Further exposure of solvent vapor led to the diffusion of vapor into the drop matrix, which caused the contact line to spread continuously until the film was formed.

Supporting video 4: The video shows 10 μl of 0.7% (w/v) 5CB solution in n-hexane was dispensed on homogeneous hydrophobic substrate. The drop underwent spreading before the solvent evaporated out of the droplet. The evaporation of the solvent and subsequent contact line instability led to the formation of an array of miniaturized LC droplets on the PDMS substrate.

Supporting video 5: The video shows Lorentz force induced motions of 5CB microdroplets on the homogeneous and hydrophobic PDMS substrate. The 5CB microdroplets were generated on a PDMS substrate following the method described in this study before the system was confined between a pair of ITO electrodes, as shown in the **Figure 7** of the main manuscript and in the video. The setup emulated the typical electrowetting EWOD experiments. Following this, the entire system was placed on a bar magnet to generate the Lorenz force. In such a scenario, when an external electric field was applied through the electrodes, near 25±1 V, the droplets elongated and touched the top electrode. This allowed the a weak current to flow though the LC droplets and the Lorenz force to set in. When the applied potential was ~90 ± 1 V, the droplets started to translate due to the thrust provided by the Lorentz force with average droplets speed of 80 ± 3.6 μm/s. The average speed of the droplets increased to 140 ± 10.8 μm/s at 95 ± 1 V, 158 ± 5 μm/s at 100 ± 1 V and 260 ± 7 μm/s at 105 ± 1 V.

Supporting video 6: The video shows the electric field induced clock and anti-clock wise motions of the LC droplet under the sole influence of electric field when the applied voltage was ~ 240 ± 2 V for a 194.5 ± 0.5 μm droplet.

Supporting video 7: The video shows the electric field induced clock and anti-clock wise motions of a number of LC droplets under the sole influence of electric field when the applied voltage was ~ 85 ± 2 V and the average diameter of the droplets were 8.96 ± 1.6 μm.

Supporting video 8: The video shows Lorentz force induced satellite LC microdroplet ejection from the primary droplets at ~ 150 ± 3 V.